ACS Photonics

Article

pubs.acs.org/journal/apchd5

Singlet-Oxygen Generation from Individual Semiconducting and Metallic Nanostructures during Near-Infrared Laser Trapping

Bennett E. Smith,[†] Paden B. Roder,[‡] Jennifer L. Hanson,[‡] Sandeep Manandhar,[‡] Arun Devaraj,[¶] Daniel E. Perea,[¶] Woo-Joong Kim,[§] A. L. David Kilcoyne,[∥] and Peter J. Pauzauskie*[,‡,⊥]

[†]Department of Chemistry and [‡]Materials Science & Engineering Department, University of Washington, Seattle, Washington, United States

[¶]Environmental Molecular Sciences Laboratory and [⊥]Fundamental & Computational Sciences Directorate, Pacific Northwest National Laboratory, Richland, Washington, United States

[§]Physics Department, Seattle University, Seattle, Washington, United States

[∥]Advanced Light Source, Lawrence Berkeley National Laboratory, Berkeley, California, United States

Supporting Information

ABSTRACT: Photodynamic therapy has been used for several decades in the treatment of solid tumors through the optical generation of chemically reactive singlet-oxygen molecules ($^1O_2$). Recently, nanoscale metallic and semiconducting materials have been reported to act as photosensitizing agents with additional diagnostic and therapeutic functionality. To date there have been no reports of observing the generation of singlet-oxygen at the level of single nanostructures, particularly at near-infrared (NIR) wavelengths. Here we demonstrate that NIR laser tweezers can be used to observe the formation of singlet oxygen produced from individual silicon and gold nanowires via use of a commercially available reporting dye. The laser trap also induces two-photon photoexcitation of the dye following a chemical reaction with singlet oxygen. Corresponding two-photon emission spectra confirms the generation of singlet oxygen from individual silicon nanowires at room temperature (30 °C), suggesting a range of applications for investigating semiconducting and metallic nanoscale materials for solid tumor photoablation.

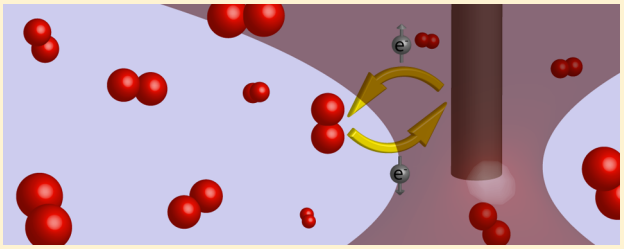

KEYWORDS: *singlet oxygen, silicon nanowires, laser tweezer, near-infrared, optical trap*

Photodynamic therapy has been used over the past two decades to clinically treat metastatic tumors through the conversion of naturally available triplet-oxygen molecules ($^3O_2$) into highly reactive singlet oxygen ($^1O_2$).[1] Singlet oxygen then reacts with a range of proteins, lipids, and nucleic acids in vivo to prevent angiogenesis within[2,3] and metastasis from solid tumors.[2,4] In this process, visible light is absorbed by an intermediate photosensitizing molecule (e.g., Photofrin[5]) to create electronic excited states, which then transfer their energy to $^3O_2$ molecules, converting them to $^1O_2$ through a triplet−triplet annihilation process.

Even though photodynamic therapy (PDT) has been studied for well over a century, it has been in clinical use only since 1993,[1] and currently there are a dozen FDA-approved photosensitizers based on small molecules.[6] Two of the primary challenges of using molecular PDT agents is their long in vivo half-lives and also their nonspecific distribution throughout the body of a patient.[5] This often leads to extended (week-long) periods of time in which a patient must avoid direct exposure to sunlight. For this reason, researchers have been studying novel ways of targeting tumor cells including micellar[7] and liposomal[8] systems, carbon nanotubes,[9] gold nanoparticles,[10] and porous silica[11] or silicon[12] materials as well as exploring new solid-state nanomaterials, including metals[13,14] and semiconductors,[15,16] as direct photosensitizers with predominant excitation wavelengths in the visible spectral window. In particular, silicon nanocrystals have been shown to sensitize singlet oxygen[17,18] and have the benefit of biodegradability[19] as opposed to inert materials such as gold nanocrystals.

The shape of nanoscale materials has also been shown to affect uptake within targeted tumor cells[20−22] due in part to the high surface-area-to-volume ratio of one-dimensional materials.[23] Furthermore, recent theoretical calculations have shown[24] that silicon nanowires can be designed to exhibit significant morphology-dependent resonances during photothermal laser heating. In this way, the shape of nanostructures can be optimized to enhance the uptake and optical absorption relative to small-molecule pharmaceuticals with fixed sizes and absorption coefficients.

The phototoxicity of silicon nanomaterials under illumination with wavelengths in the blue spectral region ($450 < \lambda < 500$ nm) has also been demonstrated.[16] Blue light, however, lies

Received: January 20, 2015
Published: March 13, 2015

DOI: 10.1021/acsphotonics.5b00022
ACS Photonics 2015, 2, 559−564

outside the near-IR (NIR) biological transparency window, resulting in a low tissue penetration depth, which has motivated recent experiments with photoexcitation of both gold nanocrystals[25,26] that can absorb light via plasmon resonance and upconverting nanocrystals[27,28] that excite surface-grafted PDT molecules following the upconversion of rare-earth ions in nanocrystalline fluoride host materials. Photoexcitation of silicon nanostructures in the NIR would increase the penetration depth and expand silicon's potential as a PDT agent.[12] We demonstrate here that NIR laser radiation (λ = 975 nm) can be used to optically excite individual silicon and gold nanowires for the local generation of $^1O_2$ within a single-beam optical trap.

RESULTS AND DISCUSSION

Silicon nanowires (SiNWs) are synthesized from p-type silicon wafers using metal-assisted chemical etching (MACE) with silver as the active etching metal.[29] High-angle annular dark-field transmission electron microscopy (HAADF TEM) was used to confirm the presence of silver domains on SiNWs following their synthesis (Figure 1a). TEM imaging also confirms that the silver nanocrystals can be removed following an aqueous etching step that dissolves silver (Figure 1b). Given that metallic nanocrystals[30] have recently been demonstrated to generate singlet oxygen, it must be implicitly ruled out that there is no residual silver to interfere with the experimental measurements.

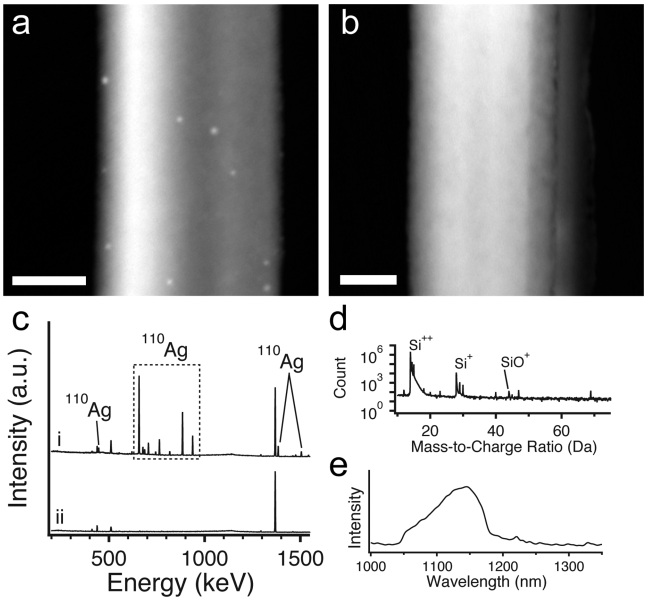

Figure 1. Compositional analysis and microstructure of silicon nanowires prepared via metal-assisted chemical etching (MACE). (a) High-angle annular dark-field image of a single silicon nanowire without silver etching, demonstrating the presence of silver deposits. Scale bar = 50 nm. (b) High-angle annular dark-field image of a silver-etched silicon nanowire with no detectable silver. Scale bar = 50 nm. (c) Neutron activation analysis of silicon nanowire array before (i) and after (ii) the silver-etching process. (d) Atom probe tomography (APT) mass spectrum from a single SiNW, demonstrating no detectable silver signal (Ag^+: 107 Da, Ag^{2+}: 53.5 Da). (e) Photoluminescence of SiNWs excited by a 975 nm laser source.

Neutron activation analysis (NAA) is a sensitive measure of metallic elemental composition and was used to analyze the residual amount of silver both with and without the silver etch (Figure 1c). The distinct gamma-ray emission from the ^{110}Ag isotope decay was used to identify and quantify the silver concentration in the SiNWs. Before silver etching, the Ag concentration is measured to be 291 ppm, whereas after silver etching the amount of Ag is below the detection limits of NAA (<100 parts per trillion).

The surface of silicon nanowires following MACE in hydrofluoric acid is expected to be hydrogen terminated; however the metal-etching step is highly oxidative and may also oxidize the surface of silicon nanowires. Fourier-transform infrared absorption spectroscopy on silicon nanowires following the silver-etching step reveals the presence of a silicon dioxide passivation layer that is also confirmed by oxygen k-edge scanning transmission X-ray absorption microscopy (see Supporting Information). Atom-probe tomography (APT) measurements on silicon nanowires further confirm the absence of silver in the bulk of the nanowires following the silver etch, as well as the presence of a surface oxide layer (Figure 1d).

Laser trapping of individual nanowires was performed using a custom instrument shown in Figure 2a. A 975 nm laser is expanded to overfill the back aperture of a 100× oil immersion objective (NA = 1.25) and then focused into a chamber with an aqueous nanowire suspension. The silicon nanowires are trapped and photoexcited by the NIR laser (Figure 2b), which is above silicon's band gap, to produce triplet excitons, as evidenced by the observation of excitonic emission from SiNWs after Ag etching (Figure 1e). The excitons then diffuse to the surface and, through a Dexter electron exchange mechanism, excite molecular oxygen in solution to the singlet state (Figure 2c) via a triplet−triplet annihilation process.[18] Singlet oxygen molecules have been reported to have a decay time of 3.7 μs in water, leading to diffusion distances on the order of 250 nm from the silicon−water interface[31] at room temperature. Singlet-oxygen excited states can also relax to their ground state through emission of a photon at 1270 nm. However, their long lifetimes at room temperature also allow for reactions with singlet oxygen sensor green (SOSG) molecules, which selectively exclude reaction with superoxide anions and peroxide,[32] to make a 1,4-endoperoxide, SOSG-EP (Figure 2d).

In addition to trapping single silicon nanowires and photoexciting triplet excitons in silicon, the laser trap also has a sufficient irradiance (~MW/cm^2) for two-photon photoexcitation (2PPE) of SOSG-EP to the electronic excited state, SOSG-EP* (Figure 3e). The green emission from SOSG-EP* can be visualized through use of a CCD camera (Figure 3a). The potential for visible photoluminescence from the porous SiNWs was eliminated as a possible source of emission by performing an identical control experiment with optically trapped SiNWs in the absence of SOSG (Figure 3b). It also has been demonstrated recently that there is negligible (<5 °C) photothermal heating of optically trapped SiNWs via analysis of their Brownian dynamics.[33]

Generation of singlet oxygen directly from SOSG has been reported previously[34] using UV or visible irradiation. An additional control experiment was performed to test for potential photogeneration of $^1O_2$ from SOSG molecules themselves at an identical NIR irradiance (Figure 3c). Clearly, the NIR source is unable to excite $^1O_2$ directly or through photosensitization of the SOSG molecule. Similarly, a final control experiment combining SOSG and SiO_2 microspheres (Figure 3d) exhibits no detectable $^1O_2$ generation at the bead's fully oxidized surface, which is expected since SiO_2 is an insulator and would not generate the excitons necessary to

DOI: 10.1021/acsphotonics.5b00022
ACS Photonics 2015, 2, 559−564

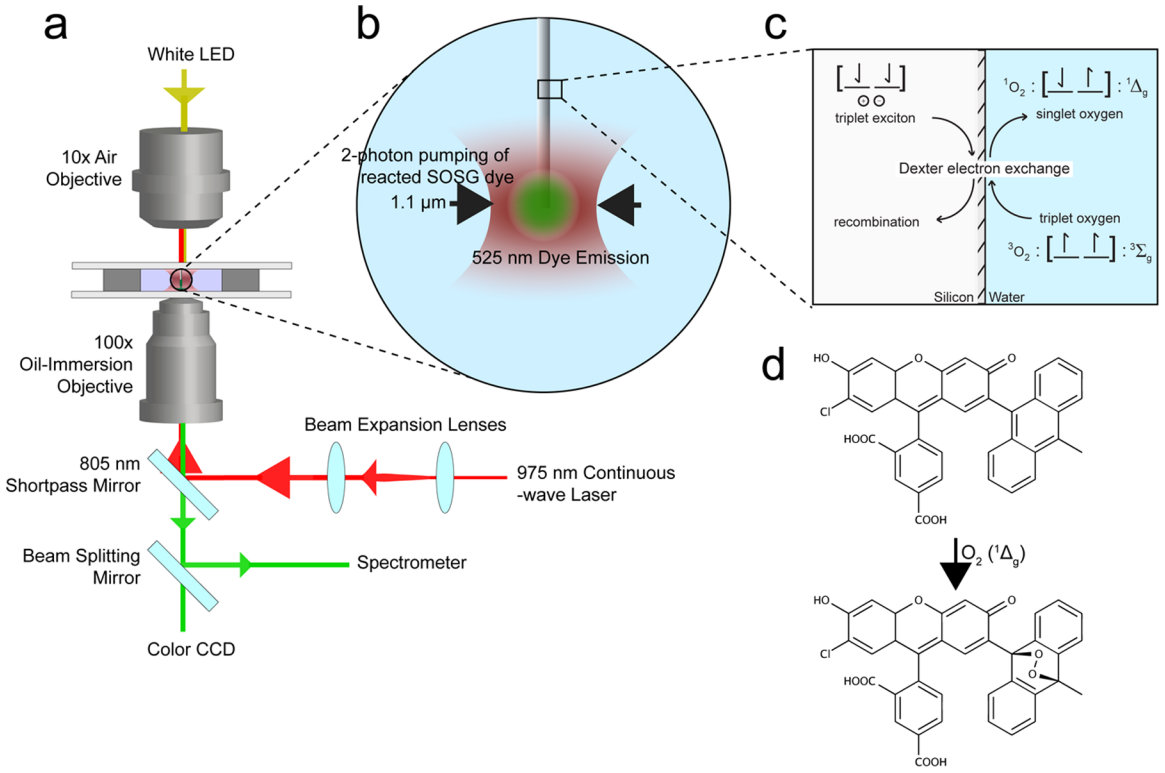

Figure 2. Schematic of laser-trapping instrument and two-photon photoexcitation of both silicon wires and SOSG-EP molecules. (a) Schematic outlining the components used in the trapping experiments. (b) Depiction of a nanowire trapped with the focused Gaussian, NIR laser (beam waist = 1.1 μm) in a solution of SOSG with localized pumping of reacted SOSG. (c) Silicon–water interface diagram showing the transfer of electrons from surface excitons in silicon to dissolved oxygen molecules. (d) Structure of SOSG before reaction with singlet oxygen and its associated endoperoxide (SOSG-EP) after reaction with singlet oxygen.

sensitize $^1O_2$. A quadratic dependence on the integrated emission from SOSG as a function of laser power is observed (Figure 3f), indicating that SOSG is excited by a two-photon mechanism.

Enhanced singlet-oxygen generation within a suspension of SiNWs is also observed at much lower laser irradiance. A cuvette with a concentrated suspension of SiNWs and SOSG was placed in the path of the 975 nm laser beam at a constant irradiance of 8 W/cm^2 (beam power = 260 mW, spot size = 2 mm) and pumped briefly at regular intervals with a low power 405 nm lamp to monitor changes SOSG-EP concentration. Comparison with a cuvette containing SOSG alone shows a significant increase in $^1O_2$ production (Figure 3g).

The approach demonstrated above for analyzing single silicon nanowires may also be extended to other nanoscale materials including noble metals. Gold nanocrystals have been shown to induce significant photothermal superheating of water when optically trapped,[35] and several recent reports have indicated that noble metal nanoparticles are capable of photogeneration of singlet oxygen.[25,26,30] In Figure 4 we show that it is possible to observe the generation of singlet oxygen from single gold nanorods that have been synthesized through electrochemical deposition within track-etched polycarbonate membranes.[37] To confirm that the observed emission is from SOSG-EP and not 2PPL from the AuNRs, a single AuNR was trapped without SOSG (Figure 4c), and long exposure micrographs showed no observable emission (Figure 4d).

CONCLUSION

We have demonstrated that a near-infrared laser trap can be used to observe the photogeneration of $^1O_2$ molecules from individual silicon and gold nanowires that are suspended within an aqueous trapping medium. To our knowledge, there have been no prior reports of observing the photosensitization of $^1O_2$ at the level of single nanostructures. Although the optical absorption coefficient of silicon at NIR wavelengths is not as high as for visible wavelengths, the use of NIR radiation allows for deeper tissue penetration. Furthermore, this work also suggests that singlet oxygen may also be generated during photothermal heating of gold and semiconductor nanostructures, including recently reported[36,38] silicon/gold composite nanostructures that have been investigated for in vivo solid tumor photothermal ablation. The NIR generation of $^1O_2$ from silicon nanowires may also affect the long-term stability of catalysts used for solar energy conversion.[39] Future studies will investigate how the efficiency of $^1O_2$ generation is affected by size-dependent morphology-dependent resonances.[24]

METHODS

Nanowire Synthesis. Silicon nanowires were synthesized using metal-assisted chemical etching methods. Briefly, a ⟨111⟩, B-doped silicon wafer with a resistivity of 11 Ω cm (Silicon Sense) is immersed in a 1:1 solution of 10 M HF/0.04 M $AgNO_3$ for 3 h, resulting in an array of vertically aligned nanowires with lengths around 10 μm and a range of diameters on the order of 100 nm. After rinsing with DI water, the etched wafers are placed into a 1:1 30% NH_4OH/28% H_2O_2 solution for 5 min to dissolve the silver film and deposits from the

DOI: 10.1021/acsphotonics.5b00022
ACS Photonics 2015, 2, 559–564

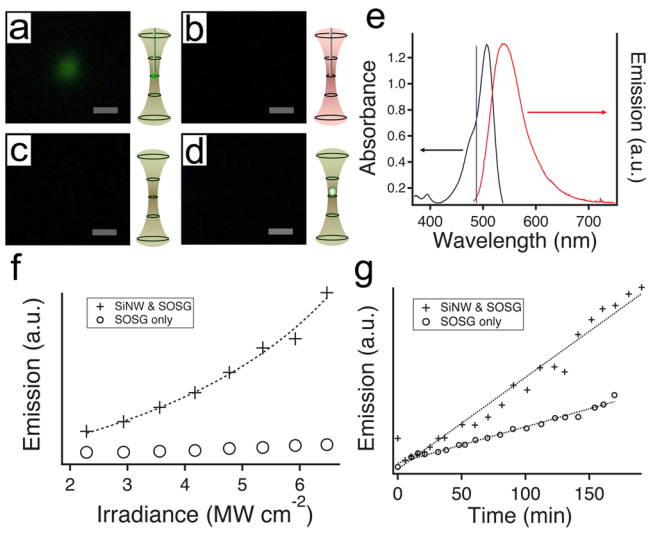

Figure 3. Singlet-oxygen ($^1O_2$) generation from silicon nanowires. Digital micrographs of (a) a single optically trapped silicon nanowire in SOSG solution, (b) a single optically trapped silicon nanowire in water alone, (c) illumination of a chamber of SOSG solution, and (d) a single optically trapped silica bead in a solution of SOSG. (e) Absorption (black) and emission (red) spectra for SOSG-EP; the blue vertical line represents the two-photon wavelength for a 975 nm trapping source. (f) SOSG-EP emission from a single trapped SiNW as a function of laser irradiance, demonstrating the nonlinearity of SOSG-EP excitation. (g) Comparison between a solution of SiNWs and SOSG and a solution of only SOSG. Both solutions were irradiated by a 975 nm laser at equal powers and, at each data point, were illuminated with a 405 nm diode to obtain the momentary emission spectrum from generated SOSG-EP. The data demonstrate an enhanced generation of singlet oxygen when SiNWs are present.

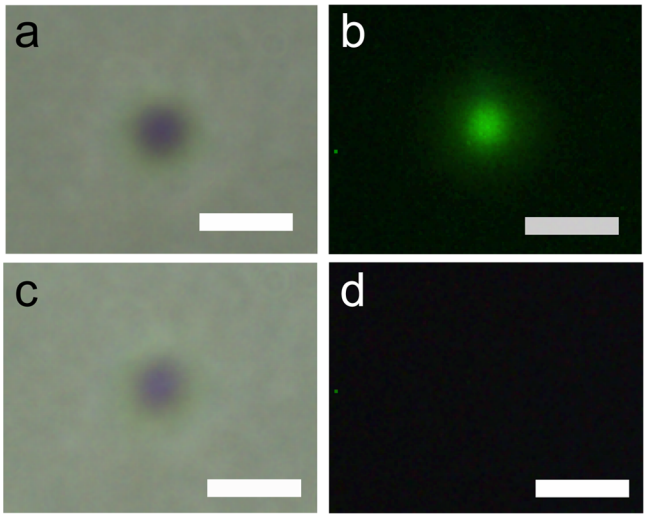

Figure 4. Singlet-oxygen ($^1O_2$) generation from a single optically trapped gold nanowire. (a) Bright-field micrograph of an electrochemically synthesized gold nanorod (AuNR) optically trapped in a solution of SOSG using the same setup used for SiNWs, diagrammed in Figure 2a. (b) Micrograph of the SOSG-EP emission from the AuNR trapped in (a). (c) Micrograph of an optically trapped AuNR in water alone. (d) Micrograph of the AuNR in (c) demonstrating no emission in the absence of SOSG. All scale bars = 2 μm.

nanowires. Gold nanowires were synthesized electrochemically using a 10 μm thick polycarbonate track etch membrane with pores of 1 μm diameter (Sterlitech) to control the dimensions of the grown nanowires. The polycarbonate membrane is subsequently dissolved in chloroform to obtain a suspension of the gold nanowires.

Single-Beam Laser Trapping. A 330 mW 975 nm laser diode (Thorlabs PL980P330J) was expanded to overfill the back aperture of a 100× Nikon oil immersion objective (NA: 1.25), which was focused into a chamber consisting of a #1 glass coverslip and a 1 mm thick glass slide with a 120 μm spacer (Grace Bio-Laboratories, #654002). Forward scattered light was focused onto a quadrant photodiode (Thorlabs, PDQ80A). Brownian analysis of a trapped particle was analyzed using custom code written using Matlab.

Neutron Activation Analysis. Compositional analysis was performed pre- and postcleaning via a TRIGA Mark II nuclear reactor. The samples were irradiated for 30 min operating at a 100 kW thermal power, 4×10^{12} neutrons/cm^2 s thermal flux, and 4.8×10^{12} neutrons/cm^2 s fast and epithermal flux. Each sample was counted while positioned near the surface of a 25 cm^2, trapezohedral, germanium, lithium-drifted semiconductor detector (Nuclear Diodes), which is constantly cooled by liquid nitrogen (77 K). Dead time between end of irradiation and start of collection was 19 h 48 min.

Atom-Probe Tomography. The needle specimens for APT were prepared by lifting out single nanowires and attaching them onto Si microtip arrays followed by Pt capping and annular milling in an FEI Helios Nanolab 600 dual-beam FIB system. Compositional analysis by APT was performed using a CAMECA LEAP 4000 XHR instrument for a total of 3.8 million ion counts. The sample temperature was maintained at 40 K, and the evaporation rate was maintained at 0.005 atom per pulse. APT analysis was conducted using a picosecond-pulsed, 355 nm UV laser (20 pJ, 100 kHz) focused onto the apex of the SiNW needle specimen.

Scanning Transmission X-Ray Microscopy (STXM). Oxygen K-edge STXM analysis was performed at the Lawrence Berkeley National Laboratory Advanced Light Source beamline 5.3.2.2. Samples for STXM analysis were prepared by drop casting a solution of SiNWs onto a lacy-carbon TEM grid and placing the grid in the STXM beamline under a one-third atmosphere of helium. Soft X-rays (250−800 eV) were focused onto the sample and rastered with a spot size of 31 nm using 25 nm Fresnel zone plates.

Singlet-Oxygen Detection. Singlet oxygen sensor green was used to detect singlet oxygen from optically trapped nanoparticles. SOSG is prepared by dissolving 100 mg in 66 μL of methanol and then diluting in Millipore (18.6 MΩ) water to obtain the appropriate concentration. SOSG-EP* emission is visualized with 20 s exposures using a Thorlabs CCD camera (DCU224C), and emission spectra were obtained by collecting emission into an Acton SpectraPro 500i spectrograph and dispersing onto a Princeton Instruments liquid-nitrogen-cooled silicon detector array.

■ ASSOCIATED CONTENT

Ⓢ Supporting Information

The Supporting Information includes additional characterization results, including NAA, FTIR, XANES, and APT. This material is available free of charge via the Internet at http://pubs.acs.org.

■ AUTHOR INFORMATION

Corresponding Author

*E-mail: peterpz@uw.edu.

DOI: 10.1021/acsphotonics.5b00022
ACS Photonics 2015, 2, 559−564

Notes

The authors declare no competing financial interest.

■ ACKNOWLEDGMENTS

This research was made possible by a grant from the Air Force Office of Scientific Research Young Investigator Program (contract FA95501210400) and start-up funding from the University of Washington. B.E.S. acknowledges support from an NIH T32 training grant (T32CA138312). P.B.R. thanks the NSF for a Graduate Research Fellowship under grant number DGE-1256082. W.J.K. acknowledges research support from the M. J. Murdock Charitable Trust and the Junior Faculty Professional Development (JFPD) grant from Seattle University. Support for nanomaterials characterization was provide by the PNNL Initiative on Materials Synthesis and Simulations Across Scales conducted under the Laboratory Directed Research and Development Program. The APT experiments were carried out through user proposal 48234 at the Environmental Molecular Sciences Laboratory (EMSL), a National Scientific User Facility located at the Pacific Northwest National Laboratory (PNNL) and supported by the U.S. DOE Office of Biological and Environmental Research. PNNL is operated by Battelle Memorial Institute for the U.S. DOE under contract DE-AC 06-76RLO 1830. The authors acknowledge Jeffrey Geuther at Kansas State University for assistance in acquiring NAA data. STXM data were acquired at beamline 5.3.2.2 at the Advanced Light Source, Berkeley, which is supported by the Director, Office of Science, Office of Basic Energy Sciences, of the U.S. Department of Energy under Contract No. DE-AC02-05CH11231. The authors also thank E. James Davis for manuscript comments and the donation of an optical spectrometer with an LN_2-cooled detector.

■ REFERENCES

(1) Dougherty, T. J.; Gomer, C. J.; Henderson, B. W.; Jori, G.; Kessel, D.; Korbelik, M.; Moan, J.; Peng, Q. Photodynamic therapy. *J. Natl. Cancer Inst.* **1998**, *90*, 889−905.

(2) Dolmans, D. E. J. G. J.; Fukumura, D.; Jain, R. K. Photodynamic therapy for cancer. *Nat. Rev. Cancer* **2003**, *3*, 380−387.

(3) Robertson, C. A.; Evans, D. H.; Abrahamse, H. Photodynamic therapy (PDT): a short review on cellular mechanisms and cancer research applications for PDT. *J. Photochem. Photobiol.* **2009**, *96*, 1−8.

(4) Bonnett, R. Photosensitizers of the porphyrin and phthalocyanine series for photodynamic therapy. *Chem. Soc. Rev.* **1995**, *24*, 19.

(5) Gilson, D.; Ash, D.; Driver, I.; Feather, J. W.; Brown, S. Therapeutic ratio of photodynamic therapy in the treatment of superficial tumours of skin and subcutaneous tissues in man. *Br. J. Cancer* **1988**, *58*, 665−667.

(6) Allison, R. R.; Sibata, C. H. Oncologic photodynamic therapy photosensitizers: a clinical review. *Photodiagn. Photodyn. Ther.* **2010**, *7*, 61−75.

(7) Lukyanov, A. N.; Gao, Z.; Torchilin, V. P. Micelles from polyethylene glycol/phosphatidylethanolamine conjugates for tumor drug delivery. *J. Controlled Release* **2003**, *91*, 97−102.

(8) Sharma, A.; Sharma, U. S. Liposomes in drug delivery: progress and limitations. *Int. J. Pharm.* **1997**, *91*, 97−102.

(9) Bhirde, A. A.; Patel, V.; Gavard, J.; Zhang, G.; Sousa, A. A.; Masedunskas, A.; Leapman, R. D.; Weigert, R.; Gutkind, J. S.; Rusling, J. F. Targeted killing of cancer cells in vivo and in vitro with EGF-directed carbon nanotube-based drug delivery. *ACS Nano* **2009**, *3*, 307−316.

(10) Vivero-Escoto, J. L.; Slowing, I. I.; Wu, C.-W.; Lin, V. S.-Y. Photoinduced intracellular controlled release drug delivery in human cells by gold-capped mesoporous silica nanosphere. *J. Am. Chem. Soc.* **2009**, *131*, 3462−3463.

(11) Lu, J.; Liong, M.; Li, Z.; Zink, J. I.; Tamanoi, F. Biocompatibility, biodistribution, and drug-delivery efficiency of mesoporous silica nanoparticles for cancer therapy in animals. *Small* **2010**, *6*, 1794−1805.

(12) Secret, E.; Maynadier, M.; Gallud, A.; Chaix, A.; Bouffard, E.; Gary-Bobo, M.; Marcotte, N.; Mongin, O.; El Cheikh, K.; Hugues, V.; Auffan, M.; Frochot, C.; Morère, A.; Maillard, P.; Blanchard-Desce, M.; Sailor, M. J.; Garcia, M.; Durand, J.-O.; Cunin, F. Two-photon excitation of porphyrin-functionalized porous silicon nanoparticles for photodynamic therapy. *Adv. Mater.* **2014**, *26*, 7643−7648.

(13) Huang, Y.-F.; Zhang, M.; Zhao, L.-B.; Feng, J.-M.; Wu, D.-Y.; Ren, B.; Tian, Z.-Q. Activation of oxygen on gold and silver nanoparticles assisted by surface plasmon resonances. *Angew. Chem., Int. Ed.* **2014**, *53*, 2353−2357.

(14) Zhao, T.; Shen, X.; Li, L.; Guan, Z.; Gao, N.; Yuan, P.; Yao, S. Q.; Xu, Q.-H.; Xu, G. Q. Gold nanorods as dual photo-sensitizing and imaging agents for two-photon photodynamic therapy. *Nanoscale* **2012**, *4*, 7712−7719.

(15) Llansola Portolés, M. J.; David Gara, P. M.; Kotler, M. L.; Bertolotti, S.; San Román, E.; Rodríguez, H. B.; Gonzalez, M. C. Silicon nanoparticle photophysics and singlet oxygen generation. *Langmuir* **2010**, *26*, 10953−10960.

(16) Xiao, L.; Gu, L.; Howell, S. B.; Sailor, M. J. Porous silicon nanoparticle photosensitizers for singlet oxygen and their phototoxicity against cancer cells. *ACS Nano* **2011**, *5*, 3651−3659.

(17) Fujii, M.; Nishimura, N.; Fumon, H.; Hayashi, S.; Kovalev, D.; Goller, B.; Diener, J. Dynamics of photosensitized formation of singlet oxygen by porous silicon in aqueous solution. *J. Appl. Phys.* **2006**, *100*, 124302−124305.

(18) Gross, E.; Kovalev, D.; Künzner, N.; Diener, J.; Koch, F.; Timoshenko, V. Y.; Fujii, M. Spectrally resolved electronic energy transfer from silicon nanocrystals to molecular oxygen mediated by direct electron exchange. *Phys. Rev. B* **2003**, *68*, 115405.

(19) Park, J.-H.; Gu, L.; von Maltzahn, G.; Ruoslahti, E.; Bhatia, S. N.; Sailor, M. J. Biodegradable luminescent porous silicon nanoparticles for in vivo applications. *Nat. Mater.* **2009**, *8*, 331−336.

(20) Champion, J. A.; Mitragotri, S. Role of target geometry in phagocytosis. *PNAS* **2006**, *103*, 4930−4934.

(21) Shi, X.; von dem Bussche, A.; Hurt, R. H.; Kane, A. B.; Gao, H. Cell entry of one-dimensional nanomaterials occurs by tip recognition and rotation. *Nat. Nanotechnol.* **2011**, *6*, 714−719.

(22) Chithrani, B. D.; Ghazani, A. A.; Chan, W. C. W. Determining the size and shape dependence of gold nanoparticle uptake into mammalian cells. *Nano Lett.* **2006**, *6*, 662−668.

(23) Barua, S.; Yoo, J. W.; Kolhar, P.; Wakankar, A.; Gokarn, Y. R.; Mitragotri, S. Particle shape enhances specificity of antibody-displaying nanoparticles. *PNAS* **2013**, *110*, 3270−3275.

(24) Roder, P. B.; Pauzauskie, P. J.; Davis, E. J. Nanowire heating by optical electromagnetic irradiation. *Langmuir* **2012**, *28*, 16177−16185.

(25) Pasparakis, G. Light-induced generation of singlet oxygen by naked gold nanoparticles and its implications to cancer cell phototherapy. *Small* **2013**, *9*, 4130−4134.

(26) Gao, L.; Liu, R.; Gao, F.; Wang, Y.; Jiang, X.; Gao, X. Plasmon-mediated generation of reactive oxygen species from near-infrared light excited gold nanocages for photodynamic therapy in vitro *ACS Nano* **2014**, *8*, 7260−7271.

(27) Wang, X.; Liu, K.; Yang, G.; Cheng, L.; He, L.; Liu, Y.; Li, Y.; Guo, L.; Liu, Z. Near-infrared light triggered photodynamic therapy in combination with gene therapy using upconversion nanoparticles for effective cancer cell killing. *Nanoscale* **2014**, *6*, 9198−9205.

(28) Kachynski, A. V.; Pliss, A.; Kuzmin, A. N.; Ohulchanskyy, T. Y.; Baev, A.; Qu, A.; Prasas, P. N. Photodynamic therapy by in situ nonlinear photon conversion. *Nat. Photonics* **2014**, *8*, 455−461.

(29) Huang, Z.; Geyer, N.; Werner, P.; de Boor, J.; Gösele, U. Metal-assisted chemical etching of silicon: a review. *Adv. Mater.* **2011**, *23*, 285−308.

(30) Vankayala, R.; Sagadevan, A.; Vijayaraghavan, P.; Kuo, C.-L.; Hwang, K. C. Metal nanoparticles sensitize the formation of singlet oxygen. *Angew. Chem., Int. Ed.* **2011**, *50*, 10640−10644.

DOI: 10.1021/acsphotonics.5b00022
ACS Photonics 2015, 2, 559−564

(31) Skovsen, E.; Snyder, J. W.; Lambert, J. D. C.; Ogilby, P. R. Lifetime and diffusion of singlet oxygen in a cell. *J. Phys. Chem. B* **2005**, *109*, 8570−8573.
(32) Flors, C.; Fryer, M. J.; Waring, J.; Reeder, B.; Bechtold, U.; Mullineaux, P. M.; Nonell, S.; Wilson, M. T.; Baker, N. R. Imaging the production of singlet oxygen in vivo using a new fluorescent sensor, singlet oxygen sensor green. *J. Exp. Bot.* **2006**, *57*, 1725−1734.
(33) Roder, P. B.; Smith, B. E.; Davis, E. J.; Pauzauskie, P. J. Photothermal heating of nanowires. *J. Phys. Chem. C* **2014**, *118*, 1407−1416.
(34) Ragás, X.; Jiménez-Banzo, A.; Sánchez-García, D.; Batllori, X.; Nonell, S. Singlet oxygen photosensitisation by the fluorescent probe singlet oxygen sensor green. *Chem. Commun.* **2009**, 2920−2922.
(35) Kyrsting, A.; Bendix, P. M.; Stamou, D. G.; Oddershede, L. B. Heat profiling of three-dimensionally optically trapped gold nanoparticles using vesicle cargo release. *Nano Lett.* **2011**, *11*, 888−892.
(36) Shen, H.; You, J.; Zhang, G.; Ziemys, A.; Li, Q.; Bai, L.; Deng, X.; Erm, D. R.; Liu, X.; Li, C.; Ferrari, M. Cooperative, nanoparticle-enabled thermal therapy of breast cancer. *Adv. Healthcare Mater.* **2012**, *1*, 84−89.
(37) Kim, W. J.; Carr, S. M. Direct contact buckling of electrochemically grown gold nanowires. *Appl. Phys. Lett.* **2005**, *87*, 173112.
(38) Su, Y.; Peng, F.; Ji, X.; Lu, Y.; Wei, X.; Chu, B.; Song, C.; Zhou, Y.; Jiang, X.; Zhong, Y.; Lee, S.-T.; He, Y. Silicon nanowire-based therapeutic agents for in vivo tumor near-infrared photothermal ablation. *J. Mater. Chem. B* **2014**, *2*, 2892−2898.
(39) Hu, S.; Shaner, M. R.; Beardslee, J. A.; Lichterman, M.; Brunschwig, B. S.; Lewis, N. S. Amorphous TiO_2 coatings stabilize Si, GaAs, and GaP photoanodes for efficient water oxidation. *Science* **2014**, *344*, 1005−1009.

DOI: 10.1021/acsphotonics.5b00022
ACS Photonics 2015, 2, 559−564